Effect of Bath Temperature on Cooling Performance of Molten Eutectic $NaNO_3$-KNO_3 Quench Medium for Martempering of Steels

K.M. PRANESH RAO and K. NARAYAN PRABHU

Martempering is an industrial heat treatment process that requires a quench bath that can operate without undergoing degradation in the temperature range of 423 K to 873 K (150 °C to 600 °C). The quench bath is expected to cool the steel part from the austenizing temperature to quench bath temperature rapidly and uniformly. Molten eutectic $NaNO_3$-KNO_3 mixture has been widely used in industry to martemper steel parts. In the present work, the effect of quench bath temperature on the cooling performance of a molten eutectic $NaNO_3$-KNO_3 mixture has been studied. An Inconel ASTM D-6200 probe was heated to 1133 K (860 °C) and subsequently quenched in the quench bath maintained at different temperatures. Spatially dependent transient heat flux at the metal–quenchant interface for each bath temperature was calculated using inverse heat conduction technique. Heat transfer occurred only in two stages, namely, nucleate boiling and convective cooling. The mean peak heat flux (q_{max}) decreased with increase in quench bath temperature, whereas the mean surface temperature corresponding to q_{max} and mean surface temperature at the start of convective cooling stage increased with increase in quench bath temperature. The variation in normalized cooling parameter t_{85} along the length of the probe increased with increase in quench bath temperature.

DOI: 10.1007/s11661-017-4267-7

I. INTRODUCTION

CONVENTIONAL quench hardening involves quenching of an austenized steel part into a quench medium. Water, mineral oils, vegetable oils, brine, and aqueous polymer solution are generally used as quench media for conventional quench hardening.[1] The heat extraction during quenching in conventional vaporizable quench media occurs in three stages, namely, vapor blanket stage, nucleate boiling stage, and convective cooling stage.[2] The heat transfer rate is very low during the vapor blanket stage, and then it increases and reaches maximum during the nucleate boiling stage. The heat transfer rate subsequently decreases to a very low value during the convective cooling stage.[3] The heat flux at the metal–quenchant interface during quenching is not only transient in nature but also spatially dependent because of the simultaneous presence of two or all three stages of cooling at the surface of the probe.[4,5] These nonuniform cooling and high heat extraction rates generally result in microstructural variation, distortion, cracking, and residual stress in the quenched part. These are major defects observed in conventional quench hardened parts.[6]

An ideal quench medium is the one that has no vapor blanket stage, very short boiling stage, and cools the part very slowly during the convective cooling stage, when austenite transforms into martensite in the steel.[7] The quench medium should transform the maximum amount of austenite into martensite by abating undesired high temperature diffusion based transformations and minimizing distortion, cracking, and residual stress in the quenched part. These qualities cannot be realized in a single quench medium, and hence, the interrupted quenching process was developed. Unlike the conventional quench hardening process that is a single-step process, the interrupted quenching process is a multistep process.

Martempering, a widely practiced industrial heat treatment process, is an example of the interrupted quenching process. Martempering involves quenching of an austenized steel part in a medium maintained at a temperature close to the martensite start temperature of the steel and held for some time. The part is then

K.M. PRANESH RAO and K. NARAYAN PRABHU are with the Department of Metallurgical and Materials Engineering, National Institute of Technology Karnataka, Surathkal, Srinivasnagar, Mangalore 575 025, India. Contact e-mails: prabhukn_2002@yahoo.co.in, knprabhu.nitk@gmail.com
Manuscript submitted September 14, 2016.
Article published online August 10, 2017

removed from the quench bath and subjected to air cooling. Holding the part in a bath maintained at a temperature of martensitic start temperature reduces the thermal gradient in the steel part, thus, reducing thermal stresses. The subsequent step of slow air cooling of the steel part ensures slow transformation of austenite into martensite, thus, reducing distortion, cracking, and residual stress in the quenched part.[8]

Martempering the heat treatment process requires a quench medium that can operate in the temperature range of 423 K to 873 K (160 °C to 550 °C) without degrading.[9] The quench bath maintained at a temperature close to the martensitic start temperature of the steel is expected to rapidly cool the austenized steel part with utmost uniformity. Rapid cooling of the austenized part avoids undesired diffusion based transformations. Nonuniform cooling induces a large temperature gradient along the surface of the steel part that ultimately acts as a cause for microstructural variation, distortion, cracking, and residual stress in the quenched part.[10] Hot oils (marquench oils), molten mixtures of alkali nitrate–nitrite salts, alkali chloride salts, alkali hydroxides and alkali carbonates, and some metal alloys are used as high-temperature quench media.[11]

Molten sodium and potassium nitrate–nitrites mixtures are the most commonly used high-temperature quench media. Generally binary or ternary mixtures of these salts are used as quench media. The melting point of these mixtures depends on their composition. Mixtures of salts having melting points ranging between 713 K and 423 K (150 °C to 440 °C) can be obtained. Dubal suggested the use of a salt mixture such that the operating temperature is at least 50 K (50 °C) greater than the melting point of the mixture.[12]

The performance of molten salt quench medium mainly depends on quench bath temperature, agitation condition, and moisture content in the quench bath.[13] In the present work, the effect of quench bath temperature on the performance of the molten eutectic mixture of $NaNO_3$-KNO_3 quench bath has been studied. 55pct$NaNO_3$-45pctKNO_3 is the eutectic mixture and thus has the lowest melting point of 493 K (220 °C).[14] Although this quench medium is widely used in industrial heat treatment applications, a study concerning the cooling performance of this quench medium has not yet been carried out.

II. EXPERIMENT

A cylindrical Inconel probe (Figure 1) of 60 mm high and 12.5 mm diameter was used to characterize the quench medium. The probe had a 5-mm length M16 thread at the top. The total height of the probe including the threaded portion was 65 mm. The M16 thread of probe was fastened to a stainless steel tube. K-type Inconel sheathed thermocouples of 1 mm diameter were inserted into 1-mm-diameter EDM drilled holes in the probe through the stainless-steel tube. The probe had five holes, one at the center drilled to a depth of 30 mm and four at 2 mm from the surface of the probe drilled to depths of 7.5, 22.5, 37.5, and 52.5 mm (depths are exclusive of the 5-mm thread at top of the probe). The thermocouples were connected to a data logger through the compensating cables. Cooling curves were obtained using a NI-9213 data logger interfaced to a PC. Temperature data were acquired at a time interval of 0.1 seconds. The instrumented probe was then heated in a vertical tubular furnace to a temperature of 1133 K (860 °C). Subsequently, the stainless-steel tube was lowered through a guide and the probe was quenched into the quench bath. A quench bath furnace was used to melt the salt mixture and to maintain the molten quench bath at required temperatures.

A. *Inverse Heat Transfer Model for Estimating Heat Flux*

An inverse heat transfer technique was used to estimate the spatially dependent transient heat flux at the metal–quenchant interface during quenching of the Inconel probe in a molten eutectic KNO_3-$NaNO_3$ mixture maintained at different quench bath temperatures. Kumar[15] developed a serial algorithm to estimate the individual boundary heat flux components, one by one, at the unknown boundary, based on the function specification method. Prabhu and Ramesh[16] used this method to determine spatially dependent heat flux transients during immersion quenching of the Inconel probe in brine and polymer media. Felde and Szenasi[17] used a particle swarm optimization method to calculate the unknown HTC function during immersion quenching. A weighted multipoint (WMP) source model that could be used to reproduce radiative heat fluxes in the near field of laminar diffusion methane-air flames was developed using the inverse method. A generalized external optimization (GEO) algorithm was used to determine and correlate WMP parameters.[18]

In the present work, the spatially dependent transient heat flux was determined using the conjugate gradient method.

Time temperature data recorded by four thermocouples located near the surface of the probe during quenching were used to estimate the spatially dependent heat flux transient at the metal–quenchant interface. Temperature data recorded at the geometric center of the probe were used to validate the estimated heat flux.

As shown in Figure 2, the heat transfer in the probe was assumed to be axisymmetric. The (r,z) coordinates at the bottom left corner of the probe were assumed to be (0,0). The surface area of the metal–quenchant interface is very large compared with the top and bottom surfaces of the probe. Heat transfer was thus assumed to be radial, and thus, the top and bottom surfaces of the probe were insulated. Heat transfer at the metal–quenchant interface was modeled as a cubic function of distance z measured from the bottom of the probe. The material removed to drill holes in the Inconel probe was less than 2 pct of the total volume of the probe. The effect of these holes on heat transfer in the probe was thus neglected. The parameters p_1, p_2 p_3, and p_4 were estimated for each time step using inverse heat transfer technique. The conjugate gradient method suggested in Reference 19 was used to estimate these parameters. An inverse heat transfer technique requires

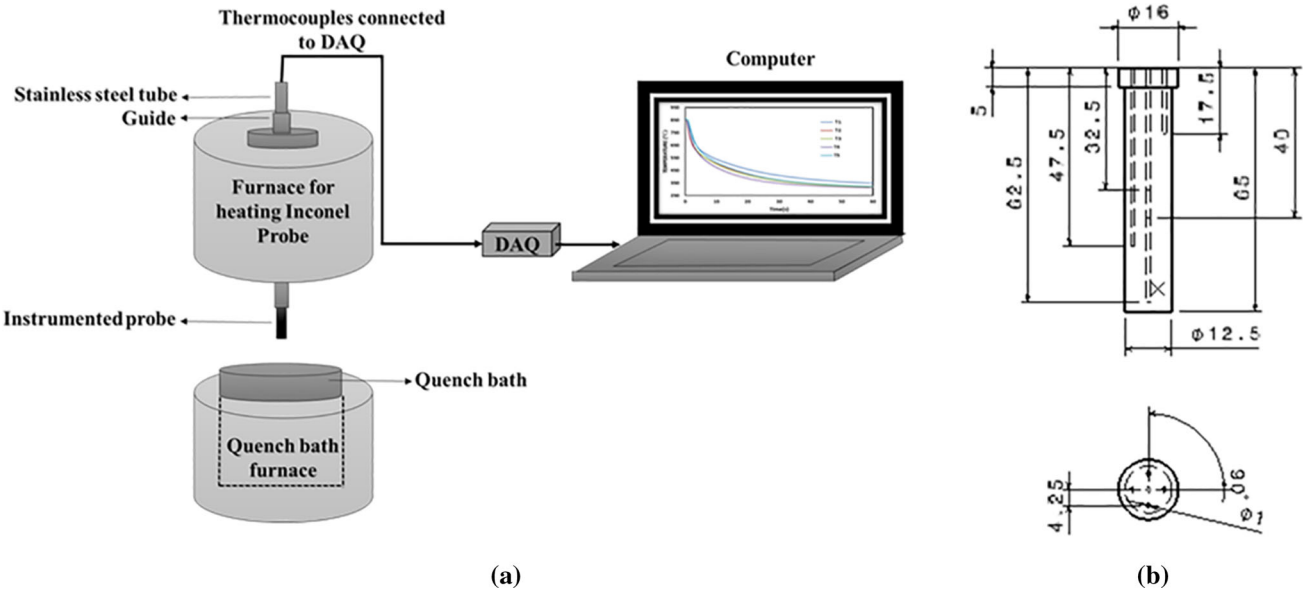

Fig. 1—(*a*) Setup for quenching experiments and (*b*) quench probe dimensions.

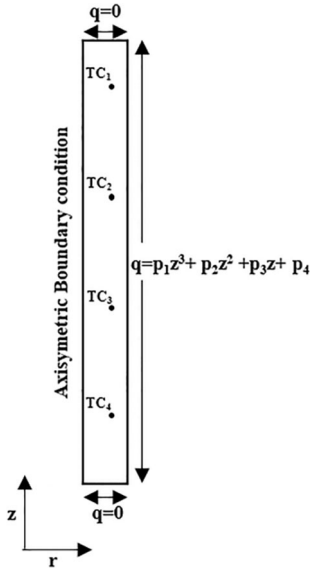

Fig. 2—Axisymmetric model of the probe used to estimate spatially dependent transient heat flux at the metal–quenchant interface.

the heat conduction equation (Eq. [1]) to be solved. A finite element method was used to solve the heat conduction equation. A 60 × 6.25-mm axisymmetric rectangular model of the probe was discretized into 6000 square elements of dimension 0.25 × 0.25 mm:

$$\frac{\partial}{\partial r}\left(kr\frac{\partial T}{\partial r}\right)+\frac{\partial}{\partial z}\left(k\frac{\partial T}{\partial z}\right)=\rho C_p\frac{\partial T}{\partial t}, \qquad [1]$$

$T\ (r,\ z,\ 0)\ =\ 1133$ K (860 °C) (Initial condition)
$q\ (0,\ z,\ t)\ =\ 0$W (Axisymmetric boundary condition)
$q\ (r,\ 0,\ t)\ =\ 0$W
$q\ (r,\ 60,\ t)\ =\ 0$W
$q\ (6.25,\ z,\ t)\ =\ p_1(t)\ z^3\ +\ p_2(t)\ z^2\ +\ p_3(t)\ z\ +\ p_4(\mathrm{t})$

The temperature data measured by thermocouples located at positions TC_1, TC_2, TC_3, and TC_4, *i.e.*, at the depths of 7.5, 22.5, 37.5, and 52.5 mm from the top end of the probe (excluding 5-mm threaded portion of the probe) were used in the inverse model. Temperature data measured by thermocouples at locations TC_1, TC_2, TC_3, and TC_4 were designated as Y_1, Y_2, Y_3, and Y_4, respectively. Temperature-dependent thermal properties of Inconel used in the FEM model are given in Table I.

The inverse problem was solved by estimating parameters $p_{1,\mathrm{ts}}$, $p_{2,\mathrm{ts}}$, $p_{3,\mathrm{ts}}$, and $p_{4,\mathrm{ts}}$ for which the objective function S_{ts} was minimized at each time step ts.

Parameters can be represented in vector form as P_{ts}:

$$P_{\mathrm{ts}}\ =\ \left[p_{1,\mathrm{ts}}\ p_{2,\mathrm{ts}}\ p_{3,\mathrm{ts}}\ p_{4,\mathrm{ts}}\right], \qquad [2]$$

$$q(P_{\mathrm{ts}},z)\ =\ p_{1,\mathrm{ts}}z^3+p_{2,\mathrm{ts}}z^2+p_{3,\mathrm{ts}}z+p_{4,\mathrm{ts}} \quad \text{where } z \text{ varies between 0 and 60 mm,} \qquad [3]$$

$$S_{\mathrm{ts}}=\sum_{i=1}^{n}\sum_{j=1}^{m}\left(Y_{i,\mathrm{ts}+j-1}-T(P_{\mathrm{ts}})_{i,\mathrm{ts}+j-1}\right)^2, \qquad [4]$$

where $Y_{i,\mathrm{ts}+j-1}$ is the temperature measured at the ith location and ts + j − 1th time step. Because temperature is measured at four locations, n = 4. $T(P_{\mathrm{ts}})$ was calculated using FEM by assuming that heat flux remains constant for the next m time steps; *i.e.*, $q\ (P_{\mathrm{ts}},\ z)\ =\ q(P_{\mathrm{ts}+1},\ z)\ =\ \ldots\ =q(P_{\mathrm{ts}+m},\ z)$.

In the present work, the number of future times steps (m) was 4.

In the vector form, Eq. [4] can be written as:

$$S_{\mathrm{ts}}=\left[Y_{\mathrm{ts}}-T\left(P_{\mathrm{ts}}^{k}\right)\right]^{T}\left[Y_{\mathrm{ts}}-T\left(P_{\mathrm{ts}}^{k}\right)\right], \qquad [5]$$

where Y and T are vectors of measured and calculated vectors written as:

Table I. Temperature-Dependent Thermal Properties of Inconel 600 Alloy (Ref. [16])

T (K) (°C)	473 K (200 °C)	523 K (250 °C)	573 K (300 °C)	623 K (350 °C)	673 K (400 °C)	723 K (450 °C)	773 K (500 °C)	823 K (550 °C)	873 K (600 °C)	923 K (650 °C)	973 K (700 °C)
k (W/mK)	16	16.9	17.8	18.7	19.7	20.7	21.7	—	25.9	—	30.1
C(J/kgK)	491	—	509	—	522	—	533	591	597	597	611
ρ(kg/m^3)	8340	—	8300	—	8270	—	8230	8190	8150	8100	8060

$$Y_{\text{ts}} = \left[Y_{1,\text{ts}}\, Y_{1,\text{ts}+2}\, Y_{1,\text{ts}+2}\, \ldots\, Y_{i,\text{ts}+j-1} \ldots\ldots\ldots\, Y_{n,\text{ts}+m}\right]^T, \quad [6]$$

$$T(P_{\text{kts}}) = \left[T_{1,\text{ts}}\, T_{1,\text{ts}+2}\, T_{1,\text{ts}+2} \ldots\ldots T_{i,\text{ts}+j-1} \ldots\ldots\ldots\, T_{n,\text{ts}+m}\right]^T. \quad [7]$$

The flow chart of the iterative algorithm used to solve the inverse problem is shown in Figure 3.

In Figure 3, β_{ts}^k, γ_{ts}^k, and d_{ts}^k are search step size, conjugation coefficient, and direction of descent respectively. J_{ts}^k is the sensitivity matrix, which was of size 16 × 4 and defined as:

$$J_{\text{ts}}^k = \left[\frac{\partial T(P_{\text{ts}}^k)}{\partial p_{1,\text{ts}}} \frac{\partial T(P_{\text{ts}}^k)}{\partial p_{2,\text{ts}}} \frac{\partial T(P_{\text{ts}}^k)}{\partial p_{3,\text{ts}}} \frac{\partial T(P_{\text{ts}}^k)}{\partial p_{4,\text{ts}}}\right]. \quad [8]$$

The partial derivatives in J_{ts}^k is calculated using:

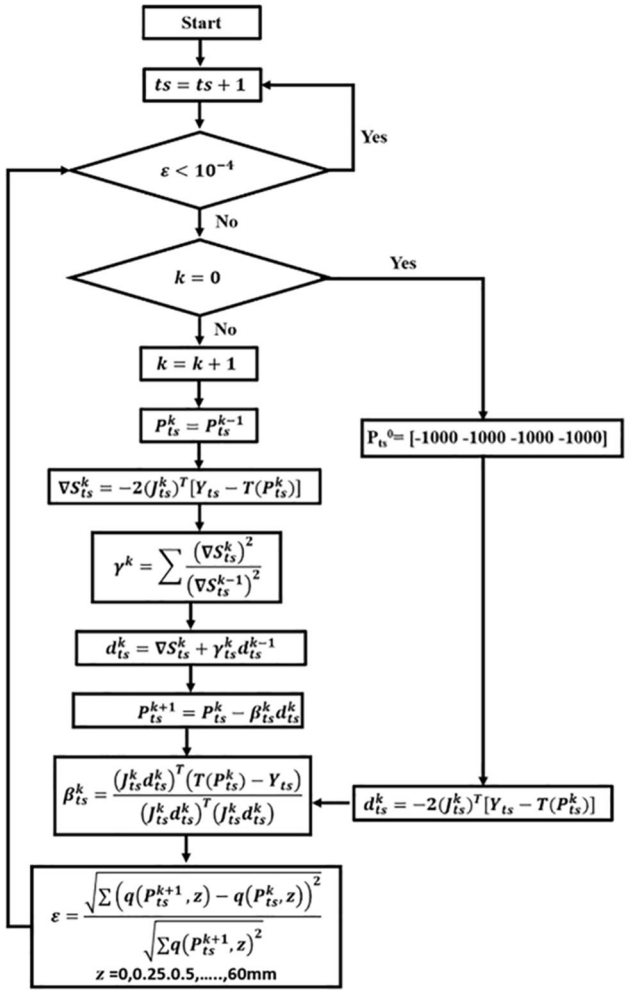

Fig. 3—Flow chart for inverse solution algorithm.

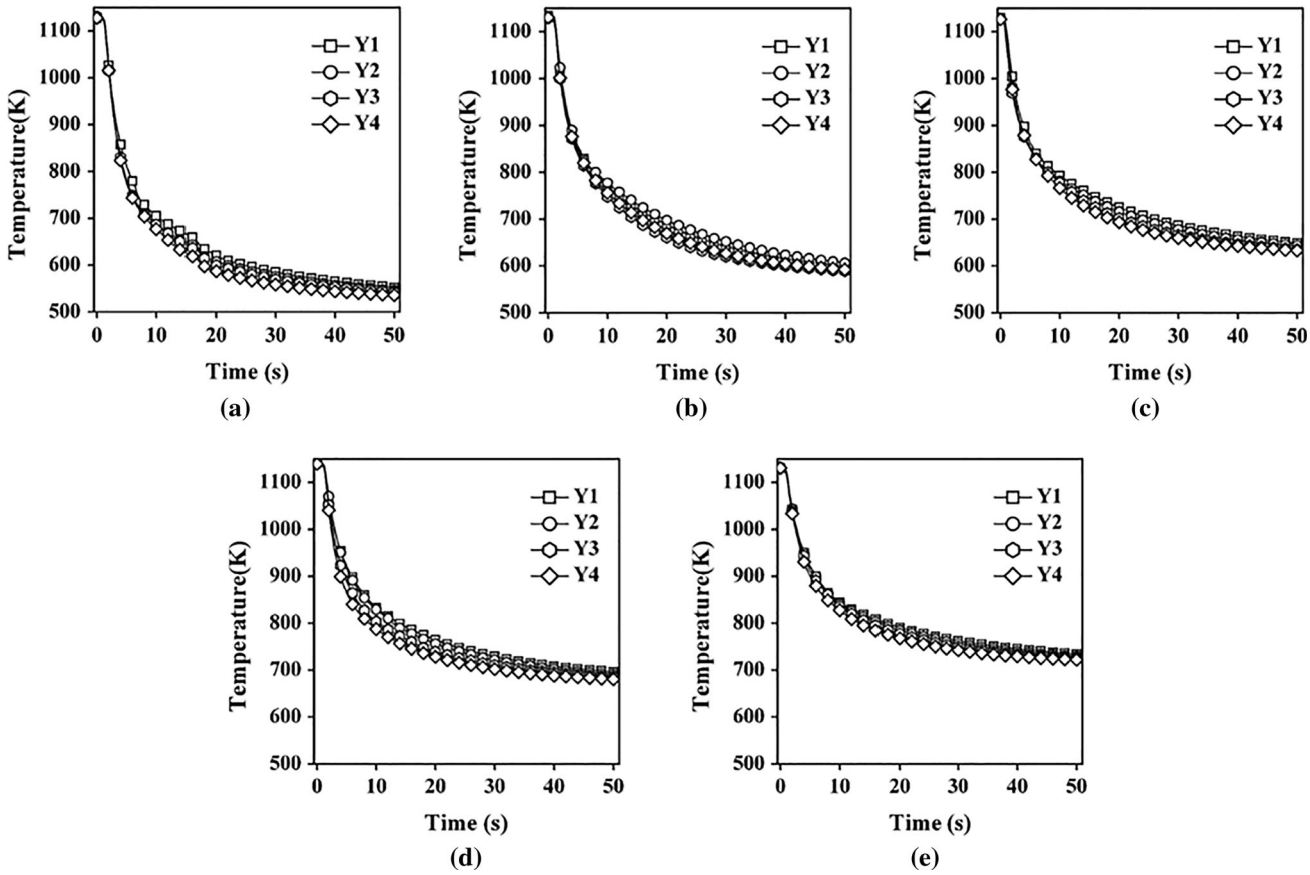

Fig. 4—Cooling curves obtained at different locations in the probe during quenching of Inconel probe in eutectic $NaNO_3$-KNO_3 quench medium maintained at (*a*) 523 K (250 °C), (*b*) 570 K (300 °C), (*c*) 623 K (350 °C), (*d*) 673 K (400 °C), and (*e*) 723 K (450 °C).

$$\frac{\partial T\left(P_{\text{ts}}^{k}\right)}{\partial p_{1,\text{ts}}} = \frac{T\left(\left[p_{1,\text{ts}}^{k}+\delta p_{1,\text{ts}}, p_{2,\text{ts}}^{k}, p_{3,\text{ts}}^{k}, p_{4,\text{ts}}^{k}\right]\right)-T\left(\left[p_{1,\text{ts}}^{k}, p_{2,\text{ts}}^{k}, p_{3,\text{ts}}^{k}, p_{4,\text{ts}}^{k}\right]\right)}{\delta P_{1,\text{ts}}}, \quad [9]$$

Here, $\delta p_{1,\text{ts}} = 10^{-4} \times p_{1,\text{ts}}$

$T([p_{1,\text{ts}} + \delta p_{1,\text{ts}}, p_{2,\text{ts}}, p_{3,\text{ts}}, p_{4,\text{ts}}])$, and $T([p_{1k,\text{ts}}, p_{k2,\text{ts}}, p_{k3,\text{ts}}, p_{k4,\text{ts}}])$ in Eq. [9] were evaluated by solving the heat conduction equation using FEM.[20] Similarly, partial derivatives of the temperature vector with respect to three other parameters, *i.e.*, $p_{2,\text{ts}}$ $p_{3,\text{ts}}$ and $p_{4,\text{ts}}$, were evaluated. The converged values of parameters P_{ts} calculated for each time step were then used to calculate spatially dependent heat flux, $q(P_{\text{ts}},z)$, using Eq. [3].

III. RESULTS AND DISCUSSION

An Inconel probe heated to 1133 K (860 °C) was quenched into molten eutectic $NaNO_3$-KNO_3 quench media maintained at a temperature of 523 K, 573 K, 623 K, 673 K, and 723 K (250 °C, 300 °C, 400 °C, and 450 °C). Time-temperature data acquired by thermocouples placed at locations TC_1, TC_2, TC_3, and TC_4 during quenching were designated Y_1, Y_2, Y_3, and Y_4, respectively, as shown in Figure 4.

Figures 5(a) through (d) show variation of parameters p_1, p_2, p_3, and p_4 with time, and Figure 5(e) shows spatially dependent transient heat flux. Parameters were calculated using the inverse heat conduction algorithm detailed earlier. Temperature data measured during quenching of the Inconel probe in the molten eutectic $NaNO_3$-KNO_3 mixture maintained at 523 K (250 °C) was used for solving the inverse heat conduction problem. Similarly, spatially dependent transient heat flux was calculated for quenching of the Inconel probe in this quench bath maintained at 573 K, 623 K, 673 K, and 723 K (300 °C, 350 °C, 400 °C, and 450 °C). It was observed that the heat flux varied considerably along the surface of the probe. The magnitude of the heat flux was observed to decrease with increase in bath temperature.

A. *Difference Between Measured and Calculated Values of Temperature*

The temperature data measured at the geometric center of the Inconel probe were not used to estimate the spatially dependent transient heat flux at the metal–quenchant interface. The temperature difference between the measured and calculated values of the temperature at the geometric center of the Inconel probe

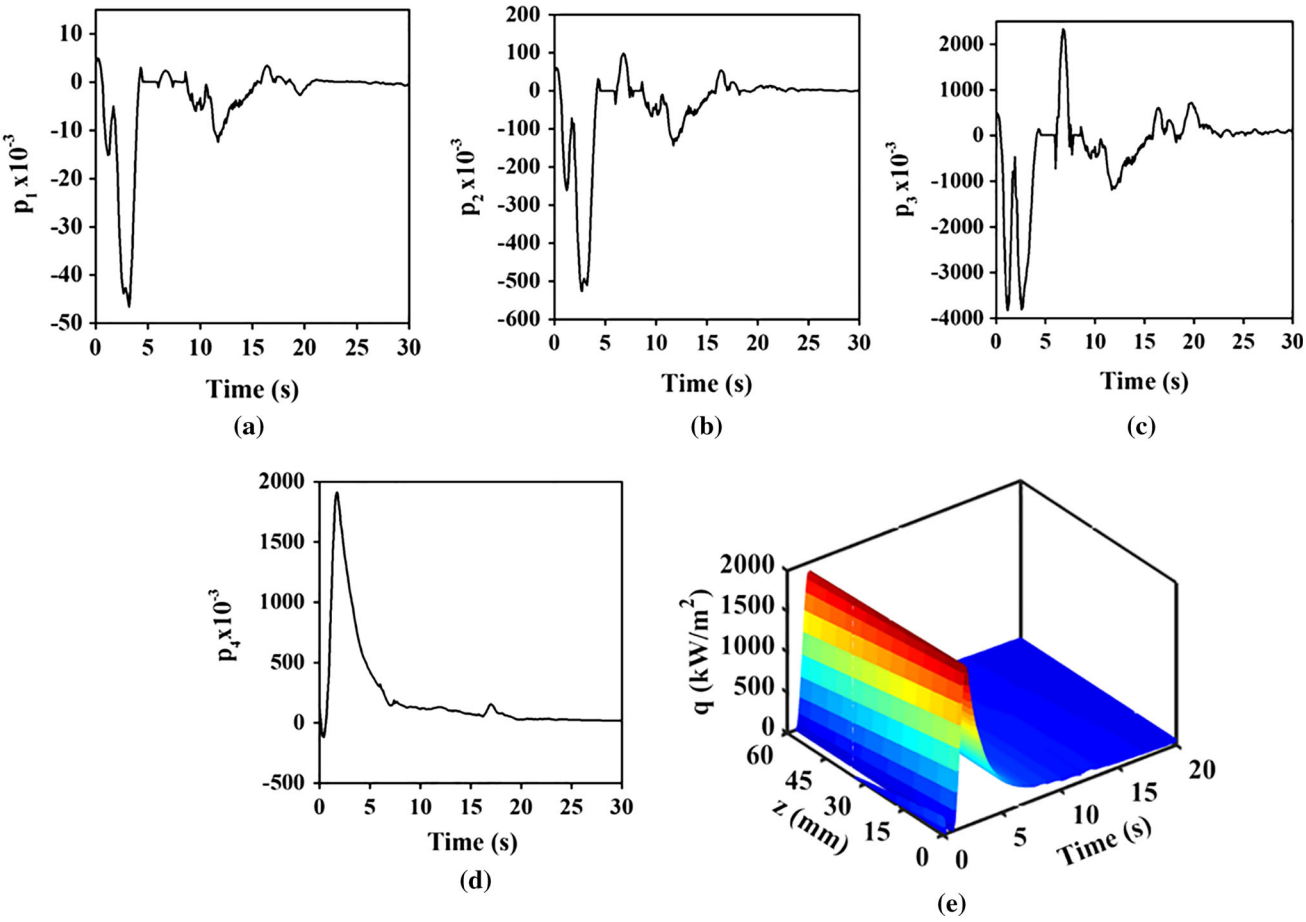

Fig. 5—Transient variation of parameter (*a*) p_1, (*b*) p_2, (*c*) p_3, and (*d*) p_4. (*e*) Spatially dependent transient heat flux calculated for Inconel probe quenched in molten eutectic $NaNO_3$-KNO_3 mixture maintained at 523 K (250 °C).

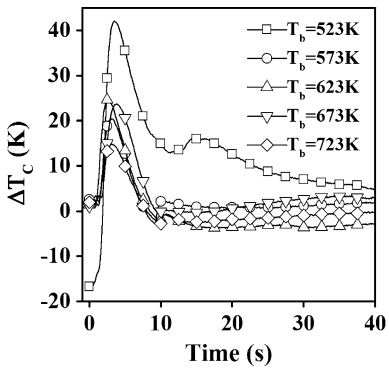

Fig. 6—Difference between measured and calculated values of temperature at geometric center of Inconel probe during quenching.

(ΔT_C) was calculated using Eq. [10]. $T_{C\text{meas}}(t)$ and $T_{C\text{calc}}(t)$ are the measured and estimated temperatures at the geometric center of the probe at time t.ΔT_C was observed to rapidly increase to a maximum value and subsequently decrease to a small value (Figure 6). ΔT_C was observed to assume both positive and negative values:

$$\Delta T_C(t) = T_{C_{\text{meas}}}(t) - T_{C_{\text{calc}}}(t) \qquad [10]$$

Similarly, ΔT was calculated as a function of time at thermocouple locations TC_1, TC_2, TC_3, and TC_4 in the Inconel probe. ΔT values were observed to follow a similar trend as that observed in the case of TC_c. Table II shows the maximum value (ΔT_{max}) and the average value (ΔT_{Avg}) calculated for absolute values ΔT. Table II shows the measured temperature corresponding to the maximum value of ΔT ($T_{\text{err-max}}$) for the Inconel probe quenched in molten eutectic $NaNO_3$-KNO_3 media maintained at different quench bath temperatures. To have ΔT_{Avg} independent values, the low values of ΔT, observed in the later part of the convection stage, ΔT_{Avg} values, were calculated for the time interval required to cool the geometric center from 1133 K (860 °C) to (T_b − 50) K. The values of ΔT_{max} and ΔT_{Avg} were observed to be considerably low at all thermocouple locations. It was thus concluded that the estimated values of q are fairly accurate.

B. *Mean Surface Heat Flux*

Spatially dependent transient heat flux and the surface temperature estimated using the inverse heat conduction method were averaged over space. The mean surface

Table II. Maximum Value and Average Value of $\Delta T$and Measured Temperature Corresponding to Maximum Value of ΔT for Inconel Probe Quenched in Molten Eutectic $NaNO_3$-KNO_3 Media Maintained Different Quench Bath Temperatures

T_b (K) (°C)		TC_1	TC_2	TC_3	TC_4	TC_C
523 K (250 °C)	ΔT_{max} (K)	9.09	12.26	9.87	12.92	42.08
	$T_{err-max}$ (K)	1116.65	719.00	1108.60	1011.38	861.81
	ΔT_{Avg} (K)	2.22	7.41	1.80	2.78	17.83
573 K (300 °C)	ΔT_{max} (K)	8.78	14.36	13.19	9.17	20.55
	$T_{err-max}$ (K)	1124.63	683.62	676.90	1116.78	899.02
	ΔT_{avg} (K)	2.82	11.40	10.17	5.28	3.14
623 K (350 °C)	ΔT_{max} (K)	9.12	3.99	7.62	4.89	24.75
	$T_{err-max}$ (K)	1119.97	1118.38	769.50	909.70	971.13
	ΔT_{Avg} (K)	5.34	3.14	3.80	6.71	5.30
673 K (400 °C)	ΔT_{max} (K)	6.08	9.78	8.54	5.58	23.72
	$T_{err-max}$ (K)	1125.14	867.14	1062.51	824.81	856.89
	ΔT_{Avg} (K)	1.76	1.89	1.40	1.58	3.86
723 K (450 °C)	ΔT_{max} (K)	1.92	2.25	2.59	2.32	4.27
	$T_{err-max}$ (K)	1123.30	1122.04	866.71	1122.44	924.03
	ΔT_{Avg} (K)	1.31	2.86	3.33	1.40	3.83

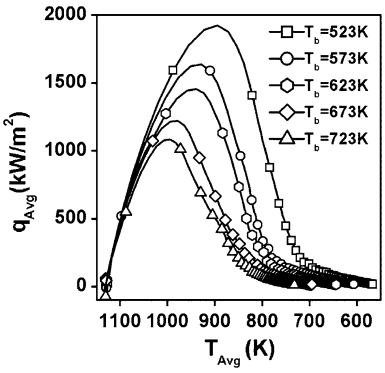

Fig. 7—Variation of mean surface heat flux with mean surface temperature at different quench bath temperatures.

temperature (T_{Avg}) and mean surface heat flux (q_{Avg}) were calculated at each time step using Eqs. [11] and [12], respectively. Integration was performed using the trapezoidal method with a step size of 0.25 mm along the z axis:

$$q_{avg}(t) = \frac{1}{l}\int_0^l q(t,z)dz \quad l = 60 \text{ mm} \;\; l = 60 \text{ mm}, \quad [11]$$

$$T_{avg}(t) = \frac{1}{l}\int_0^l T(t, r_{max}, z)dz \quad r_{max} = 6.25\,\text{mm}, \; l = 60\,\text{mm}. \quad [12]$$

Analysis of mean heat flux and mean surface temperature gives an estimate of the variation of transient heat flux. Figure 7 showed that irrespective of quench bath temperature, the curves followed the same trend. Initially, heat flux rapidly increased from zero to a maximum value, and then it decreased. The rate of decrease of heat flux was high initially but decreased at the later stage. Unlike vaporizable conventional liquid quench media (water, oil, *etc.*), which exhibit three stages of cooling during quenching, namely, vapor blanket stage, nucleate boiling stage, and convective cooling stage, molten eutectic KNO_3-$NaNO_3$ quench medium exhibits only the nucleate boiling and convection stages.

The molten salt medium boils when it initially comes in contact with the surface of the probe at a high temperature. It was observed that the peak mean heat flux (q_{max}) decreased with increase in quench bath temperature (T_b). The mean surface temperature of the probe (T_{max}) corresponding to q_{max} increased with increase in quench bath temperature. Equations [13] and [14] were obtained by linear regression (Figures 8(a) and (b)). These equations relate q_{max} and T_{max} with the quench bath temperature, respectively. The points in Figure 8 correspond to the values of q_{max}, T_{max} and T_{conv} obtained for different trials.

$$q_{max} = -4.14T_b + 3992.07, \quad [13]$$

$$T_{max} = 0.47T_b + 664.4. \quad [14]$$

The sudden change in slope of the curve observed in Figure 7 indicates the transition of the cooling mechanism from the boiling stage to the convective cooling stage. It was observed that the convective cooling stage starts when heat flux reduces below a critical value (q_{conv}), which was observed to be 185.5 ± 26.78 kW/m^2 irrespective of quench bath temperature. q_{conv} is the minimum heat flux required to boil the molten $NaNO_3$-KNO_3 quench bath. Further, it was observed that the mean surface temperature at which the convective cooling stage starts (T_{conv}) increased with increase in quench bath temperature. Equation [15] relates T_{conv} and T_b (Figure 8(c)):

$$T_{conv} = 0.73T_b + 339.15. \quad [15]$$

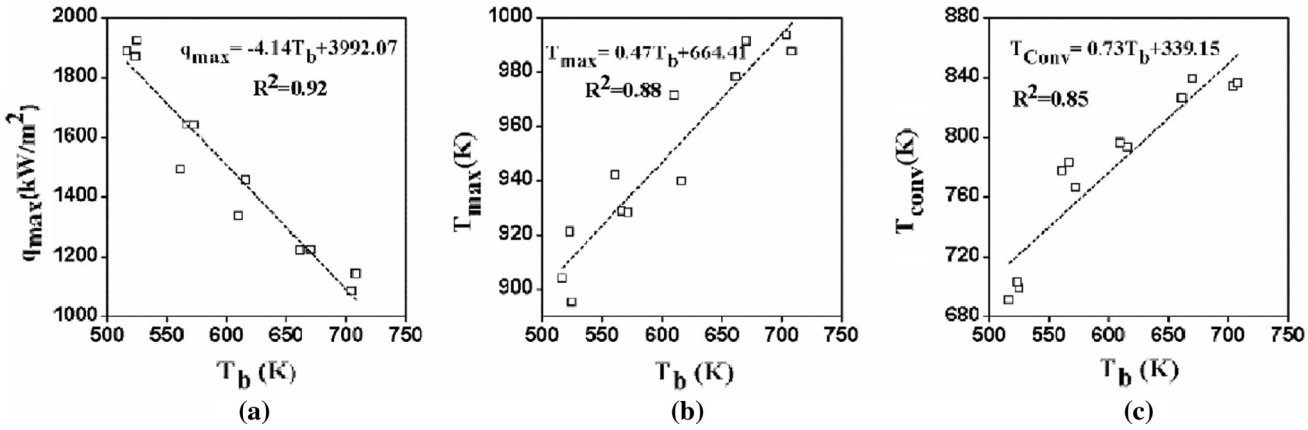

Fig. 8—Linear regression model relating (*a*) q_{max} and T_b (*b*) T_{max} and T_b (*c*) T_{conv} and T_b.

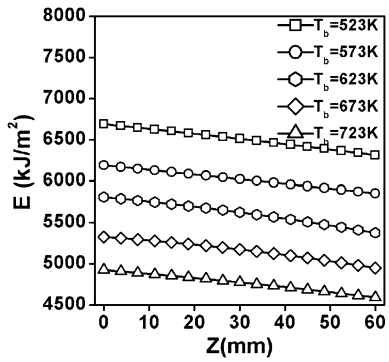

Fig. 9—Variation of heat energy removed per unit area with distance.

C. *Spatial Dependenc of Heat Transfer*

The metal–quenchant interfacial heat flux estimated using the inverse method significantly varied with the distance (z) measured from the bottom of the probe. The cumulative effect of the transient nature of the heat flux at a given location was evaluated by calculating spatially dependent heat energy extracted per unit area. Heat energy extracted per unit area (E), from the surface of the probe, was calculated as a function of distance using Eq. [16]. The trapezoidal method with a step size of 0.1 seconds was used to evaluate the integral:

$$E(z) = \int_0^{t\_max} q(t,z)dt \quad t_{max} = 40 \text{ s.} \qquad [16]$$

As observed in Figure 9, energy extracted from the bottom section of the probe was higher compared to that extracted from the top section of the probe at all quench bath temperatures. This variation in heat energy extracted along the surface of the probe was attributed to the significantly large difference in the heat transfer characteristics along the surface of the probe.

The time required to cool from 1273 K to 773 K (800 °C to 500 °C), known as t_{85}, is a characteristic cooling time, which is relevant for prediction of phase transformation during quenching of most structural steels. Smoljan[21] used t_{85} as a cooling parameter in conjunction with the chemical composition of steel to predict the phase microstructure distribution in a 41Cr4 (DIN) steel shaft. It is to be noted that a lower value of t_{85} results in higher hardness and *vice versa*.

For each quenching experiment, the t_{85} values were obtained at each node of the axisymmetric model of the Inconel probe and were normalized by dividing them with the maximum value of t_{85}. The normalization of t_{85} values facilitates the comparison of distribution of t_{85} values irrespective of their magnitude. Figure 10 shows the distribution of normalized t_{85} in the axisymmetric model of the Inconel probe quenched in the eutectic $NaNO_3$-KNO_3 quench medium maintained at different bath temperatures.

It was observed that the variation of normalized t_{85} along the length of the probe increased with increase in the bath temperature of the quench medium. The values of normalized t_{85} were observed to be lower in the bottom part of the probe compared to the top part of the probe. The nonuniform distribution of t_{85} was attributed to the variation of heat transfer characteristics along the surface of the probe.

A regression model was developed to predict the t_{85} value at the geometric center of an Inconel probe quenched in molten eutectic $NaNO_3$-KNO_3 media maintained at any given quench bath temperature (Figure 11). The t_{85} values linearly increased with increase in quench bath temperature. The regression model is presented as:

$$t_{85c} = 0.0734T_b + 33.24. \qquad [17]$$

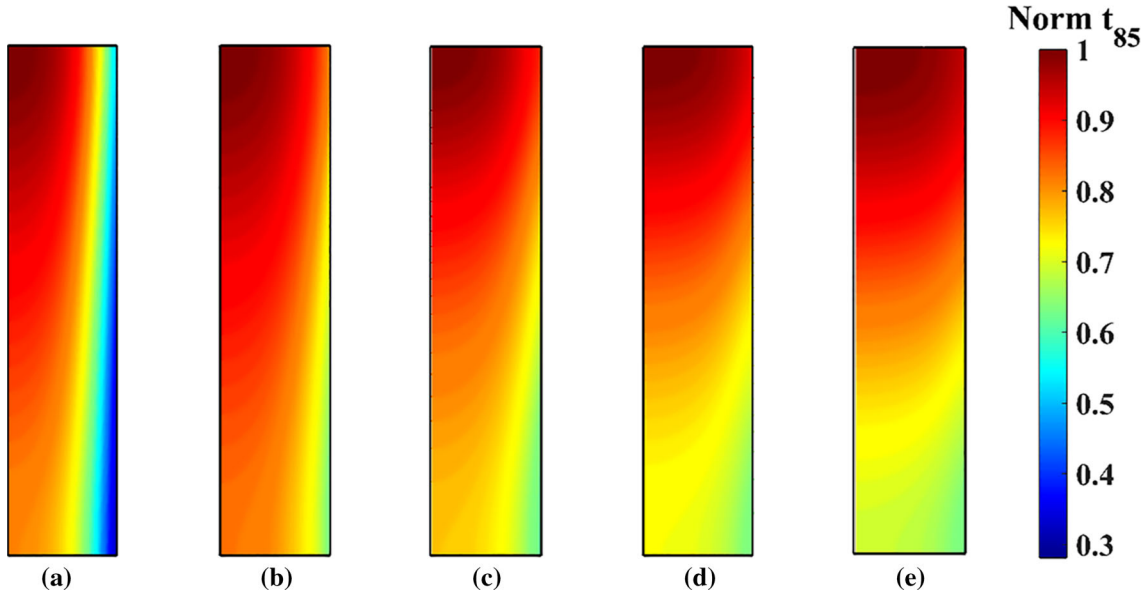

Fig. 10—Normalized t_{85} distribution in axisymmetric hot Inconel probe quenched in eutectic $NaNO_3$-KNO_3 quench medium maintained at (*a*) 523 K (250 °C), (*b*) 570 K (300 °C), (*c*) 623 K (350 °C), (*d*) 673 K (400 °C), and (*e*) 723 K (450 °C).

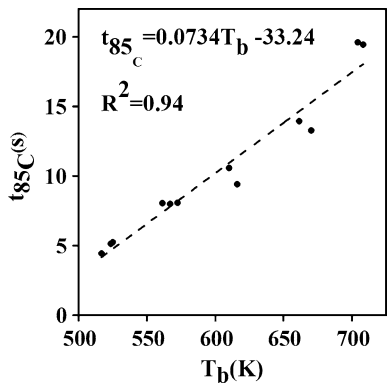

Fig. 11—Regression model to predict t_{85} value at the geometric center of an Inconel probe quenched in molten eutectic $NaNO_3$-KNO_3 media maintained at any given quench bath temperature.

IV. CONCLUSION

Based on the results and discussion, the following conclusions were drawn:

(1) Spatially dependent transient heat flux for quenching of a hot Inconel probe in molten eutectic $NaNO_3$-KNO_3 quench medium, maintained at different bath temperatures, was calculated using inverse heat conduction method based on the conjugate gradient technique. The calculated heat flux transients were validated by comparing estimated and measured temperature data at the geometric center of the probe.

(2) Heat transfer during quenching occurred in two stages, namely, the boiling and convective cooling stages.

(3) The mean peak heat flux (q_{max}) during the boiling stage and the corresponding mean surface temperature (T_{max}) decreased and increased with quench bath temperature, respectively. Linear regression equations were formulated to predict the values of q_{max} and T_{max} for a given quench bath temperature.

(4) The convective stage that followed the boiling stage was observed to start when the mean surface heat flux dropped below 185.5 ± 26.78 kW/m^2. The mean surface temperature corresponding to the start of the convective cooling stage (T_{conv}) was found to increase with increase in quench bath temperature.

(5) The variation of heat energy removed per unit area with distance suggested that the heat transfer at the bottom part of the probe was higher compared with that in the top part of the probe. Consequently, higher values of normalized t_{85} were observed at the bottom part of the probe compared with that at the top part of the probe.

(6) The variation of normalized t_{85} values along the length of the probe increased with increase in the bath temperature of the quench medium.

(7) A linear regression model was developed to predict the t_{85} value at the geometric center of an Inconel probe quenched in molten eutectic $NaNO_3$-KNO_3 medium maintained at any given quench bath.

NOMENCLATURE

r	Radial direction in polar coordinate system (mm)
z	Axial direction in polar coordinate system (mm)
q	Spatially dependent transient heat flux (kW/m^2)

p_1, p_2, p_3, p_4	Parameters in cubic equation for estimation of q
P	Vector representation of parameters p_1, p_2, p_3, and p_4
k	Thermal conductivity (W/mk)
ρ	Density (kg/m^3)
C	Specific heat (J/kgK)
t	Time (s)
Y	Measured temperature vector
T	Calculated temperature vector
S	Objective function
β	Search step size
γ	Conjugation coefficient
d	Direction of descent vector
J	Jacobian matrix
ε	Convergence criterion
T_{Cmeas}	Temperature measured at the geometric center of the probe (K)
T_{Ccalc}	Temperature calculated at the geometric center of the probe (K)
ΔT	Difference between measured and calculated values of temperature
q_{Avg}	Spatially dependent heat flux averaged over space (kW/m^2)
T_{Avg}	Mean surface temperature (K)
T_{b}	Temperature of quench bath (K)
q_{max}	Peak mean heat flux (kW/m^2)
T_{max}	T_{Avg} corresponding to q_{max} (K)
q_{conv}	Value of q_{Avg} at the start of convective cooling stage (kW/m^2)
T_{conv}	T_{Avg} at which convective cooling stage starts (K)
E	Energy extracted per unit area (kJ/m^2)
t_{85}	Time of cooling from 1273 K to 773 K (800 °C to 500 °C) (s)

SUBSCRIPTS

ts	Time step
m	Number of future time steps
n	Number of thermocouples
i	Location number
j	Future time step number

SUPERSCRIPT

k	Iteration number

REFERENCES

1. B. Liscic, H.M. Tensi, L.C.F. Canale, and G.E. Totten: *Quenching Theory and Technology*, 2nd ed., CRC Press, Boca Raton, FL, 2010, pp. 359–443.
2. G.E. Totten, C.E. Bates, and N.A. Clinton: *Handbook of Quenchants and Quenching Theory*, ASM International, Materials Park, OH, 1993, pp. 291–338.
3. K.N. Prabhu and P. Fernandes: *J. Mater. Des.*, 2007, vol. 28 (2), pp. 544–50.
4. Stitch A., Tensi H.M. (1990) *VII International Congress for Heat Treatment of Metals*, Moscow, pp. 136-50.
5. V.U. Nayak and K.N. Prabhu: *J. Mater. Eng. Perform.*, 2016, vol. 25 (4), pp. 1474–80.
6. C. Şimşir and C.H. Gür: *Comput. Mater. Sci.*, 2008, vol. 44, pp. 588–600.
7. Herring D.H: The HERRING GROUP Inc. Professional Support Services, doctor.com/documents/Vacuum Oil Quenching Tech.pdf, access date 25/07/2016..
8. ASM Handbook Committee: *ASM Handbook Volume 4 Heat Treating*, ASM International, Materials Park, OH, 1991, pp. 324–66.
9. Park Thermal International Corp., 1996.
10. G.E. Totten, M. Howes, and T. Inoue: *Handbook of Residual Stress and Deformation of Steel*, Materials Park, OH, ASM International, 2002, pp. 248–330.
11. G.P. Dubal: *Adv. Mater. Process.*, 1999, vol. 156 (6), pp. H23–8.
12. Dubal G.P. (2003) *Heat Treating Progress* 3.
13. Reid B (1996) Park Thermal International Corp.
14. J.W. Raade and D. Padowitz: *SolarPaces Conf.*, 2010, vol. 1 (510), pp. 1–8.
15. T.S.P. Kumar: *NumerHeat Transfer, Part B*, 2004, vol. 45 (6), pp. 541–63.
16. R. Gopalan and K.N. Prabhu: *Metall Mater. Trans. B*, 2014, vol. 45B (4), pp. 1355–69.
17. I. Felde and S. Szenasi: *Int. J. Microstruct. Mater. Prop.*, 2016, vol. 11 (3/4), pp. 288–300.
18. R.B. Miguel, I.M. Machado, F.M. Pereira, P.R. Pagot, and F.H.R. França: *Int. J. Heat Mass Transfer*, 2016, vol. 102, pp. 816–25.
19. M.N. Özisik and H.R.B. Orlande: *Inverse Heat Transfer: Fundamentals and Applications*, Taylor and Francis, New York, 2000, pp. 35–115.
20. K. Babu and T.S.P. Kumar: *J. ASTM Int.*, 2012, vol. 9 (5), pp. 1–12.
21. B. Smoljan: *J. Mater. Process. Technol.*, 2006, vol. 175 (1–3), pp. 393–97.